Physico-mechanical Properties of *Sapindus mukorossi* Seed

Xiaopeng Bai,[a,b] Daochun Xu,[a,b,*] Wendi Sun,[a] and Ziyu Diao [a]

This work characterized physical and mechanical properties of *Sapindus mukorossi* seed to explore the mechanical behaviors of the seed during compression in a roll crusher. A new method that combines simulations and calculations with experimental data obtained using a three-dimensional optical measurement system for the measurement of the Poisson ratio and elasticity modulus of the hollow-sphere seed hull was proposed. The modulus of elasticity was derived from a mechanics formulation and verified in a computer simulation based on experimental data. Scanning electron microscopy and energy-dispersive spectrometry were conducted to reveal the mesostructure and components of the seed hull. The results revealed that the average densities of the *S. mukorossi* seed shell and kernel were respectively 1.49 and 1.07 × 10^3 kg/m^3, the average Poisson's ratio was 0.185, and Young's modulus ranged from 1.3 to 0.3 GPa. These values had little dispersion, demonstrating both the consistency of the processing techniques and the stability of the material properties. The given properties of the *S. mukorossi* can be used as a theoretical basis for the optimized processing of this biomass material. The proposed method provides a new direction in the study of the mechanical properties of biomaterials.

DOI: 10.15376/biores.18.1.1008-1024

Keywords: Sapindus; Mechanical properties; Mesostructure; Elemental composition; Finite element analysis

*Contact information: a: School of Technology, Beijing Forestry University, Beijing 100083, China; b: Key Lab of State Forestry Administration on Forestry Equipment and Automation, Beijing 100083, China; * Corresponding author: xudaochun@bjfu.edu.cn*

INTRODUCTION

Sapindus mukorossi, a deciduous tree that grows to a height exceeding 20 m and belongs to the Sapindaceae family, originates from South China, the Indochina Peninsula, and India (Wang *et al.* 2021). *S. mukorossi* has two layers of outer cover. One is the fruit pulp and the other is the seed shell, and both protect the inner soft kernel (see Fig. 1). The outer pericarp extract, a source of natural surfactants, is a product with great washing capacity and detergency and is particularly suited to the food and pharmaceutical industries (Yin *et al.* 2011; Yekeen *et al.* 2020). Meanwhile, pericarps have been found to have inhibitory effects on tumor necrosis factor (Morikawa *et al.* 2010) and to have many pharmacological activities, including anti-anaphylaxis, anti-inflammatory, and phlegm elimination activities (Shah *et al.* 2017; Liu *et al.* 2019). Moreover, the *S. mukorossi* kernel has an oil content as high as 40.7% and contains rich phytosterols (β-sitosterol) and a large amount of medium-chain monounsaturated fatty acids, and it thus has potential in the biodiesel industry (Basu *et al.* 2015; Sun *et al.* 2017). Biodiesel production from *S.*

mukorossi oil would provide a renewable, sustainable, and environmentally friendly source of energy (Chakraborty and Baruah 2013).

Fig. 1. Fruit and seeds of *S. mukorossi*: a) exposed seed and b) seed structure

Nevertheless, the seeds of *S. mukorossi* are not used as much as the fruit pulp in factories, mainly because of the hard hulls and glazed seed surface that make seed milling difficult and energy-consuming work. Currently, *S. mukorossi* is usually manually processed, heated and dried, and then broken in a traditional iron mortar pestle (Sunanda *et al.* 2013). Roll crushers have also been widely used for breaking the seeds, but most roll crushers have a low crushing efficiency and high cost. Techniques of optimizing the simulation of the crushing process have been extensively investigated. For instance, a mathematical model has been developed to reproduce the performance of the double-roll crusher of a urea granulation circuit and to optimize the gap setting to meet specific requirements of the crushed-particle size distribution (Cotabarren *et al.* 2008). Similarly, a new breakage–agglomeration model for a double-roll crusher has been established to reproduce particle behaviors and to predict the product size distributions of coal breakage products (Kwon *et al.* 2012). The cited studies found that mechanical properties are vital factors in modeling and analysis. The practical purpose of studying mechanical properties is to help researchers understand the situation of the forced shell when crushed and to improve the crushing efficiency. Moreover, knowledge of these properties is essential for the proper design and operation of agriculture/forestry machinery and equipment for drying, hulling, storage, and oil extraction (Santalla and Mascheroni 2003b). Furthermore, morphological knowledge and the distribution of morphological features are critical for the drying, peeling, transport, and mechanical extraction of oil (Santalla and Mascheroni 2003a). De Figueiredo *et al.* (2011) reported the importance of porosity in the design of solvent-based extraction methods.

In summary, fracture properties, such as the fracturing force, depend on many mechanical properties, porosity properties, and morphological characteristics and are critical to the design of a seed-breaking machine and seed post-processing equipment (Selvam *et al.* 2014; Munder *et al.* 2017). However, research on *S. mukorossi* has been limited to the application of the seeds. The mechanical properties, morphological structure, and elemental composition of *S. mukorossi* seed hulls have not yet been explored. Previous studies have shown that the finite element method (FEM) can be used to simulate the loading process of agricultural materials and analyze the inherent mechanical properties and damage law of agricultural materials (Cai *et al.* 2011; Tu *et al.* 2015). Van Vinh *et al.* (2022) developed an improved first-order shear deformation theory and FEM for static bending and buckling analysis of bidirectional functionally graded porous plates. Garg *et al.* (2022) predicted the elemental stiffness matrix of FG nanoplates, showing that the accuracy in predicting the behavior of the structure using FEM was improved by

optimizing the precision of the evaluation of the stiffness matrix. Cuong-Le *et al*. (2022) established a size-dependent numerical solution adopting strain gradient theory and an isogeometric finite element formulation. Kumar *et al.* (2021) improved the predictions of the free-vibration response for a porous graded nanostructure by adopting a closed-form equation and the FEM based on trigonometric higher-order shear deformation theory in conjunction with nonlocal theory. Alimirzaei *et al.* (2019) applied the FEM to the nonlinear analysis of a viscoelastic micro-composite beam with geometrical imperfections to calculate the nonlinear bending, critical buckling load, and natural frequencies of the micro-composite beam. However, there has been no analysis of the mechanical properties of *S. mukorossi* using the FEM.

The objectives of the present work were to fill the knowledge gap of mechanical properties of the seed hull of *S. mukorossi* by investigating and evaluating the density, modulus of elasticity, and Poisson's ratio of the seed hull. A proposed method of applying an optical deformation technique and a strain measurement system (ARAMIS) was adopted to obtain Poisson's ratio, whereas the modulus of elasticity was derived from a mechanics formulation and verified through computer simulation using experimental data. The mesostructure and elemental composition of *S. mukorossi* seeds were investigated using scanning electron microscopy (SEM) and energy-dispersive spectrometry (EDS) analyses.

EXPERIMENTAL

Seed Materials

The raw material used in this study was *S. mukorossi*, a species of Chinese origin, obtained from Fujian Province (26°13′48″N; 117°36′36″E), China, in May 2020. The seeds, which matured in September, were collected at the full fruiting stage and then dried in the sun.

The seeds were first separated manually from the pericarps. The seeds were then crushed into broken shell materials using a vise to single out the shell. The broken shell and kernel were then each separated into three groups (s1, s2, s3 and k1, k2, k3) and weighed on an electronic balance to measure the weight, and the volume was determined *via* drainage, at an approximate temperature of 20 °C. Experiments were conducted three times and the reported results are average values of the experimental data.

Poisson's Ratio

To study the transversal and longitudinal deformation of *S. mukorossi* seed when compressed, an ARAMIS 3D system (GOM, MBH, Germany) was placed in front of an electronic universal tester (EUT, Zwick Armaturen Gmbh, Ennepeta, Germany) (Fig. 2). ARAMIS is an optical deformation and strain analysis system and is ideally suited to measure, with high temporal and local resolution and high accuracy, the three-dimensional deformation and strain in real components and material specimens (Peterka and Uranský 2011). The EUT and ARAMIS 3D system used in the static compression test belong to the Central Laboratory of Strength and Vibration at Tsinghua University (Beijing, China).

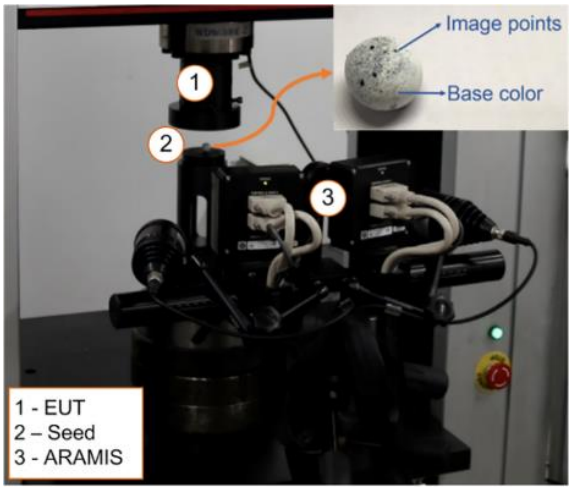

Note: Six groups of seeds were evenly sprayed with white paint as the base color and then sprayed with black paint from a long distance to produce obvious spots as image points for data collection in the static compression experiment.

Fig. 2. Experimental devices and specimen

The seeds were slowly compressed by the EUT, and the displacement and strain in different zones of the seed were recorded by the ARAMIS system (Fig. 2). The image points on the specimens were recorded by the optical arrangement of two digital charge coupled device cameras with high resolution (Panasonic Electric, Beijing, China). Together with the photogrammetry, a geometric model that allows the transformation from image points to object points was established (Hamouda *et al.* 2015). In the static or dynamic loading procedure, the three-dimensional deformation and surface strain of specimens were calculated or recorded using the object points.

The process of compression was divided into several stages in the calculation. The EUT and ARAMIS system continuously output data until the specimens broke apart. Poisson's ratio is obtained by simple calculation in the case that the transverse strain and longitudinal strain are known,

$$\mu = -\varepsilon_x/\varepsilon_y \quad (1)$$

where μ is Poisson's ratio of the seed, ε_x is the transverse strain, and ε_y is the longitudinal strain (all being dimensionless).

Modulus of Elasticity

Derivation of mechanical formulas

This study used a model of elastic–plastic contact between a sphere and rigid flat put forward by Kogut *et al.* (2002) to obtain the elasticity modulus of a *S. mukorossi* seed by simplifying the seed as a sphere. The stress state of the model has high similarity with the stress state of the specimen in the experiment.

The interface and contact area with radius *a* (Fig. 3) correspond to a contact load *P*. The deformation of the seed in the direction of compression, ω (mm) is,

$$\omega = z + \mu_z \quad (2)$$

where *z* (mm) is the vertical distance between the boundary point of the contact area and the rigid flat and μ_z (mm) is the critical interface.

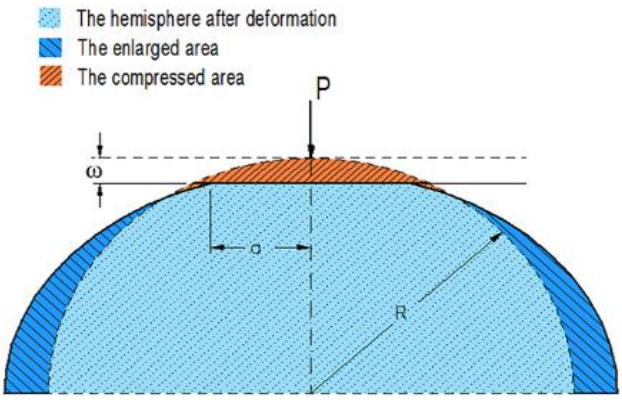

Note: Solid and dashed lines respectively show the situation after and before deformation.

Fig. 3. A deformable hemisphere, with radius R, pressed by a rigid flat

Hertz contact theory defines z and u_z as

$$z = \alpha^2[1/(2R_1) + 1/(2R_2)], \quad (3)$$

$$\mu_Z = k \cdot \iint q(\tilde{\alpha}) d_x d_\varphi, \quad (4)$$

and the variable quantity k (MPa^{-1}) is defined as,

$$k = \frac{(1-\mu_1)}{(2\pi G_1)} + \frac{1-\mu_2}{2\pi G_2} = (1-\mu^2)/(\pi E_1) + (1-\mu^2)/(\pi E_2) \quad (5)$$

where R_1 (mm) and R_2 (mm) are respectively the radii of the specimen and the metal flat plate of the EUT; μ_1 and μ_2 are respectively the Poisson ratios of the specimen and metal flat plate of the EUT; and E_1 (MPa) and E_2 (MPa) are respectively the Young's moduli of the specimen and metal plate of the EUT.

For a rigid flat metal plate with radius R_2, $E_2 \rightarrow \infty$.

The Hertz solution for the elastic contact between a sphere and flat provides the radius of the contact surface,

$$\alpha = [0.75\pi \times kP/(2\beta)]^{1/3}, \quad (6)$$

$$\beta = (R_1 + R_2)/(2R_1R_2) = 1/(2R_1), \quad (7)$$

where α (mm) is the radius of the contact area and β (mm^{-1}) is a constant.

Geometric analysis suggests a contact area of,

$$s = \pi\alpha^2 = \pi \times [R^2 - (R - \Delta L/2)^2] \quad (8)$$

where ΔL is the deformation (mm) measured in the experiment and R (mm) is the radius of the deformable hemisphere.

The modulus of elasticity is estimated from Eq. 8. In this study, statistics were taken over a timed interval to reduce the computation load for the modulus of elasticity. IBM SPSS software 21 (IBM, Armonk, USA) was used for the collection and analysis of the statistics. The interval was 12 s except for the first group of specimens, for which the interval was 60 s because the compression of the specimens was slow. The calculations revealed that the modulus of elasticity decreases as R_1 increases, as verified in subsequent simulation.

Simulation Analysis

The three-dimensional modeling software Solid Edge (SIEMENS, 2020 Berlin and Munich, Germany) was used to establish a model of the *S. mukorossi* seed in accordance with actual seed sizes. To reproduce the size of the seed as truly as possible, after the seeds were placed reasonably, they were photographed alongside a ruler as a reference. The photograph was then imported into the photo-editing program Photoshop (Adobe Systems, CC2019, San Jose, USA) to determine the size of the seed's shape for the particular camera view. In the modeling, the model was simplified as a sphere without a hilum or white hair on top, avoiding adversely affecting the final calculation precision and allowing for easier finite element analysis and better computational efficiency. The seeds were cut at both ends to produce tiny planes that allowed fixed support and pressure to be loaded (Fig. 4).

The established geometric model of *S. mukorossi* seed was imported into the static structural module of the ANSYS Workbench 14.5 (ANSYS, Pittsburgh, Pennsylvania, USA) using the Para solid format, and a mesh was then generated with body sizing. The material parameters were defined in accordance with the density and Poisson's ratio obtained in the experiment and the modulus of elasticity conjectured from mechanical formulas of the contact model. The deformation generated in simulation was compared with deformation statistics of the static compression test to confirm the agreement of results of the modulus of elasticity between theory and experiment.

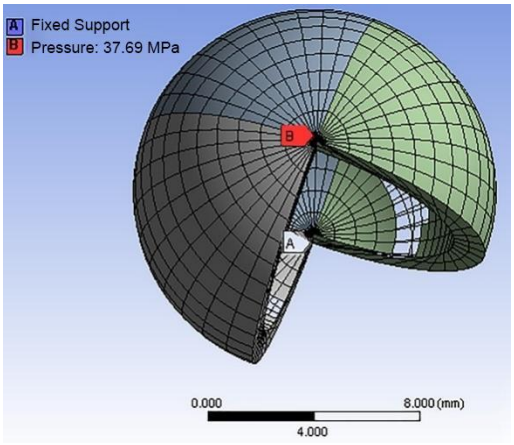

Fig. 4. Mesh and settings of the *S. mukorossi* seed model

Mesostructure and Elemental Analysis

A layer of broken shell samples was sputter-coated with gold for 300 s in a sputter coater (IB-3, Eiko, Japan) and imaged on an SEM system (Zeiss, Oberkochen, Germany) belonging to the National Center for Electron Microscopy in Beijing at Tsinghua University. The glazed outside surface, cross-section, inner surface, and hilum of seed shell fragments were observed and photographed through SEM at 2000×, 150×, 500×, and 500× magnification respectively. The samples were also sputter-coated with carbon for probing with an SEM-EDS system (Zeiss, Oberkochen, Germany). A small area on the outside surface of a seed shell was randomly selected for qualitative and quantitative analysis of the composition of elements.

RESULTS AND DISCUSSION

Intrinsic Density

The seed intrinsic density is mainly used to determine the maturity and plumpness as well as to speculate regarding the composition of the seeds. *S. mukorossi* seed kernels are rich in oil, and a riper and plumper seed tends to have lower density. The seed shell mainly comprises stone cells formed by cellulose and lignin, and its compact structure provides a high intrinsic seed density. The intrinsic densities of most seeds of agricultural crops are approximately 1.10 to 1.50 × 10^3 kg/m^3 (corn: ~1.11 to 1.22 × 10^3 kg/m^3, wheat: ~1.20 to 1.53 × 10^3 kg/m^3, soy: ~1.14 to 1.28 × 10^3 kg/m^3, rice: ~1.04 to 1.18 × 10^3 kg/m^3).

The test results for the intrinsic density of the seed hull and kernel are presented Table 1. The average intrinsic density of the *S. mukorossi* seed shell obtained by measurement was 1.49 × 10^3 kg/m^3, whereas that of the kernel was 1.07 × 10^3 kg/m^3, which indicates that the hulls and kernel can be separated using a liquid with density between 1.49 and 1.07 × 10^3 kg/m^3; *e.g.*, anhydrous glycerol, whose intrinsic density is 1.26 × 10^3 kg/m^3.

Table 1. Sample Number, Volume, and Intrinsic Density of the Seed Hull and Kernel

Sample No.	Mass (g)	Volume (mL)	Intrinsic Density (10^3 kg/m^3)	
			Value Per Sample	Average Value
s1	1.87	1.20	1.56	1.49
s2	1.15	0.80	1.44	
s3	2.21	1.50	1.47	
k1	0.72	0.70	1.03	1.07
k2	1.23	1.10	1.12	
k3	1.38	1.30	1.06	

Poisson's Ratio

Following the experiment, the computer directly output cloud diagrams of deformation. Several stages of the deformation of one group of samples are shown as Fig. 5.

The figure shows that deformation increased with compression of the seeds. However, the overall deformation was small, with the maximum longitudinal deformation being 0.15 mm and the lateral deformation not exceeding 0.05 mm. Moreover, the deformation of the seed shell during compression was not identical for different parts of shell, with deformation on both sides of the seed being appreciable while that of the center section being small. Even the lateral deformation of the central area was not completely consistent.

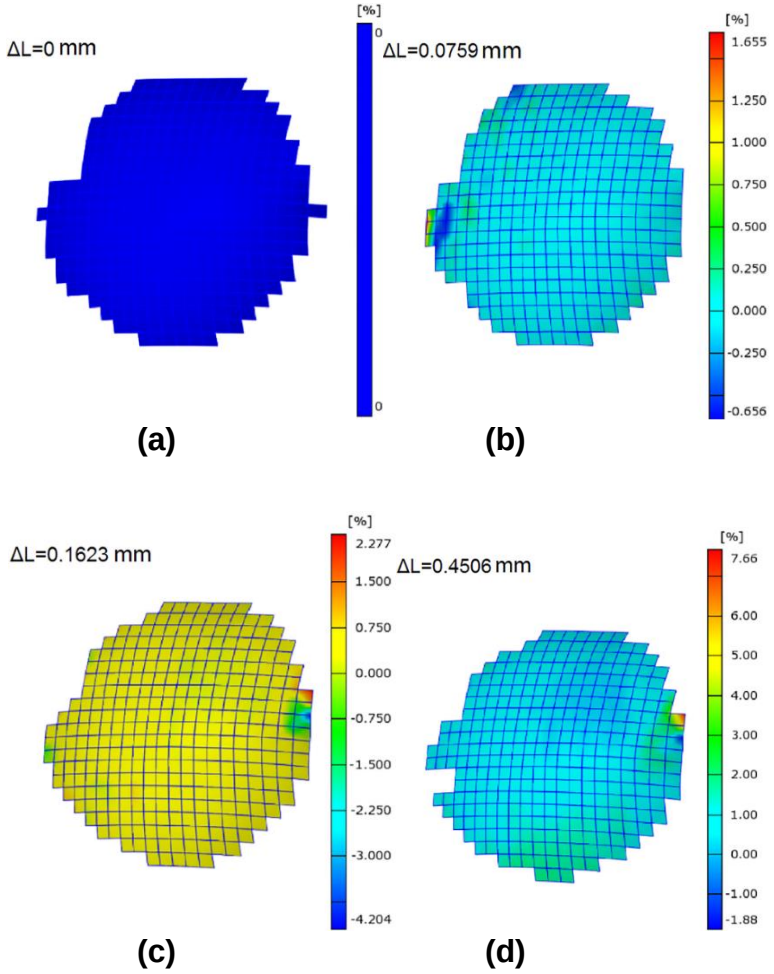

Fig. 5. Transverse deformation process for a) Δ*L* = 0, b) Δ*L* = 0.0759 mm, c) Δ*L* = 0.1623 mm, and d) Δ*L* = 0.4506 mm

Figure 6 presents the average Poisson ratios and standard deviations for six groups of samples. It can be seen that the Poisson ratio of the seeds for a given compression process fluctuated around a certain value. The average value for the six groups was approximately 0.185. The low Poisson's ratio reveals that the lateral deformation was not as large as the longitudinal deformation and that the lateral stiffness was greater than the longitudinal stiffness. Therefore, in the compression process, the seed material had better lateral bending resistance *versus* its neutral axis.

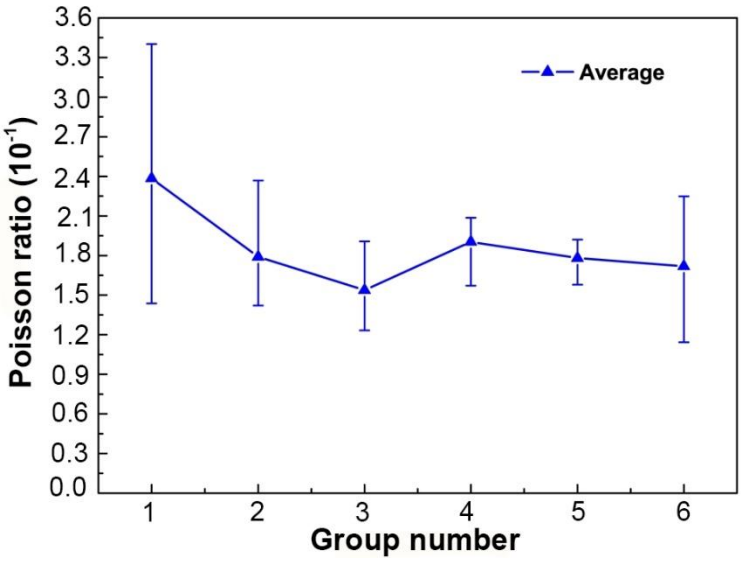

Fig. 6. Poisson ratio (with bars showing the standard deviation) for six groups of samples

The fluctuation of the Poisson ratio between groups was within 0.08. The fluctuation within the first group, from 0.14 to 0.35, was significant (standard deviation/error bars: 0.11). This result is possible due to the time interval of the data analysis for the first group of specimens being longer than that for the other groups. Although there was no obvious variation in the elasticity modulus during the time interval, the fluctuation of lateral deformation per unit time was considerable.

Modulus of Elasticity

Simulation analysis clearly revealed the deformation process and total deformation of the shell (Fig. 7). The same trend was seen for the total deformation in the experiment and simulation.

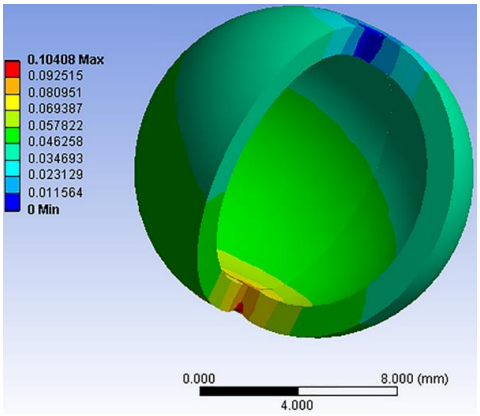

Fig. 7. Results of total deformation of the shell in the finite element analysis

The strain obtained from the theoretical model and simulation was compared with that obtained in the experiment. The simulation and experiment results of the deformation are compared in Fig. 8.

It can be seen that the deformation (ΔL) in the simulation and experiment increased roughly linearly with the compression time. These results suggest that the deformation had

a certain degree of linearity. Moreover, the slope of deformation in the experimental data over time was slightly greater than that in the simulation. The slopes in the simulation and experiment results were less different before 36 s. Furthermore, the simulation values were initially close to the experimental values, with the range of error being less than 0.05 mm, but the gap increased to as much as 0.3 mm under increasing pressure. This is presumably because the seed hulls deformed during the experiment and became increasingly difficult to model. Additionally, the simplified seed modeling resulted in certain deviations from the *S. mukorossi* seed properties. The simulation results thus included aberrations. Additionally, the simulation results show that the deformation may differ even for the same distance of the measuring points from the pressure point, which verifies the asymmetry of the internal organization and structure.

The modulus of elasticity is shown at different stages for the six groups in Fig. 9. It can be seen that the modulus of elasticity continued to change throughout the compression process, from 1.3 to 0.3 GPa, meaning that the shell of the *S. mukorossi* seed stiffness gradually decreased. This phenomenon may be due to the gradual destruction of the cell wall of the seed shell during the compression of the *S. mukorossi* seed. Moreover, the variation trend of the elastic modulus was the same for each group, and the deviation between groups was relatively small. The result shows a high degree of consistency between repeated experimental runs.

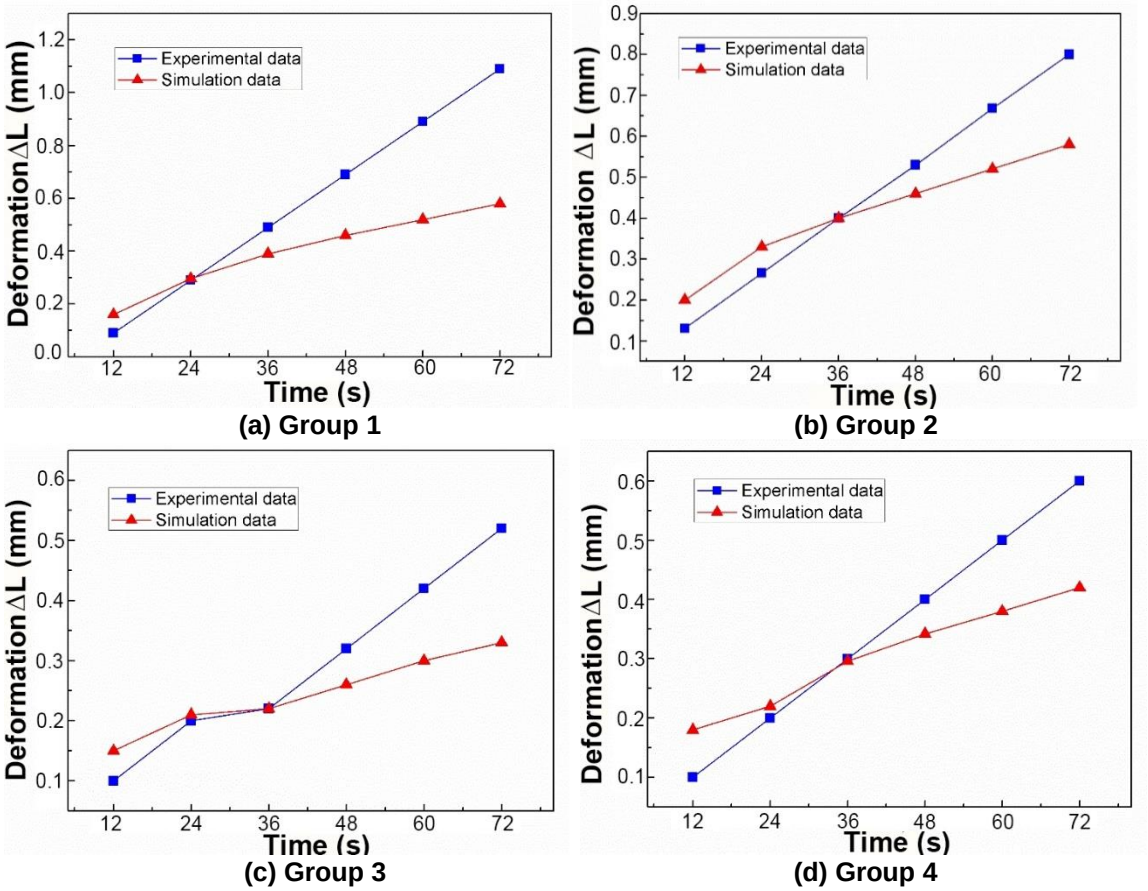

Fig. 8. Comparisons of simulation results and experiment data of a) Group 1, b) Group 2, c) Group 3, and d) Group 4

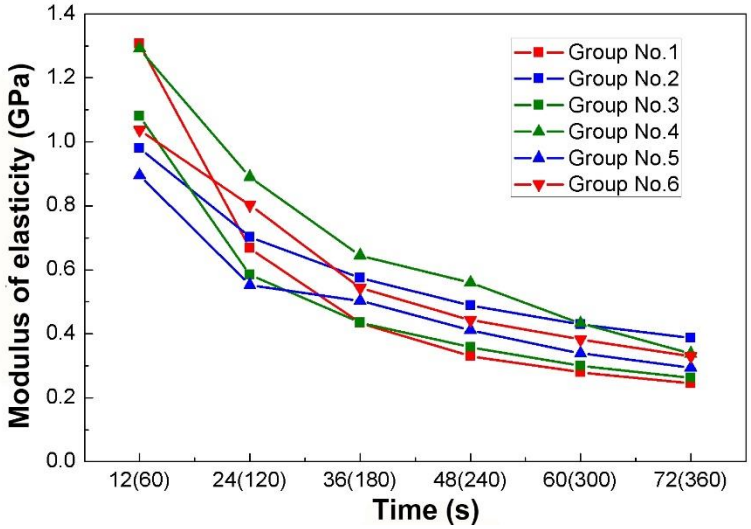

Note: The timings of the first group are given in parenthesis

Fig. 9. Modulus of elasticity of the six groups at different stages

The difference in the elastic modulus between groups may be due to the different seed sizes used in each group, as found by Abbaspour-Fard *et al.* (2012). The descent rate gradually decreased, possibly because the change in the modulus of elasticity was mainly controlled by the volume, and the volume changes with increasing temperature (Fan *et al.* 2017). It is also considered that the specimen may have material nonlinearities that affect the elasticity modulus.

Each group had the same trend of the modulus of elasticity at each stage, except for the first group, which had the largest change from the first stage to the sixth stage. This is because the experiment was conducted with much longer time intervals for the first group. Even so, the difference between groups in each stage was not more than 0.4 GPa.

Mesostructure and Elemental Composition

S. mukorossi seeds have a harder and thicker protective barrier than most plant seeds (Fabiana *et al.* 2016). The mesostructure analysis of the exterior surface and cross-section performed in the present study showed a compact cellular structure of the seed shell, which protects the kernel from the outside.

The outermost layer comprised lignified flake-like stone cells, which are tiny and compact (Fig. 10a) and are the strongest barrier of the seed. The cells had an average size of 10 to 12 μm^2 and there were tiny cracks, approximately 2 to 3 μm in width, between the flake-like cells.

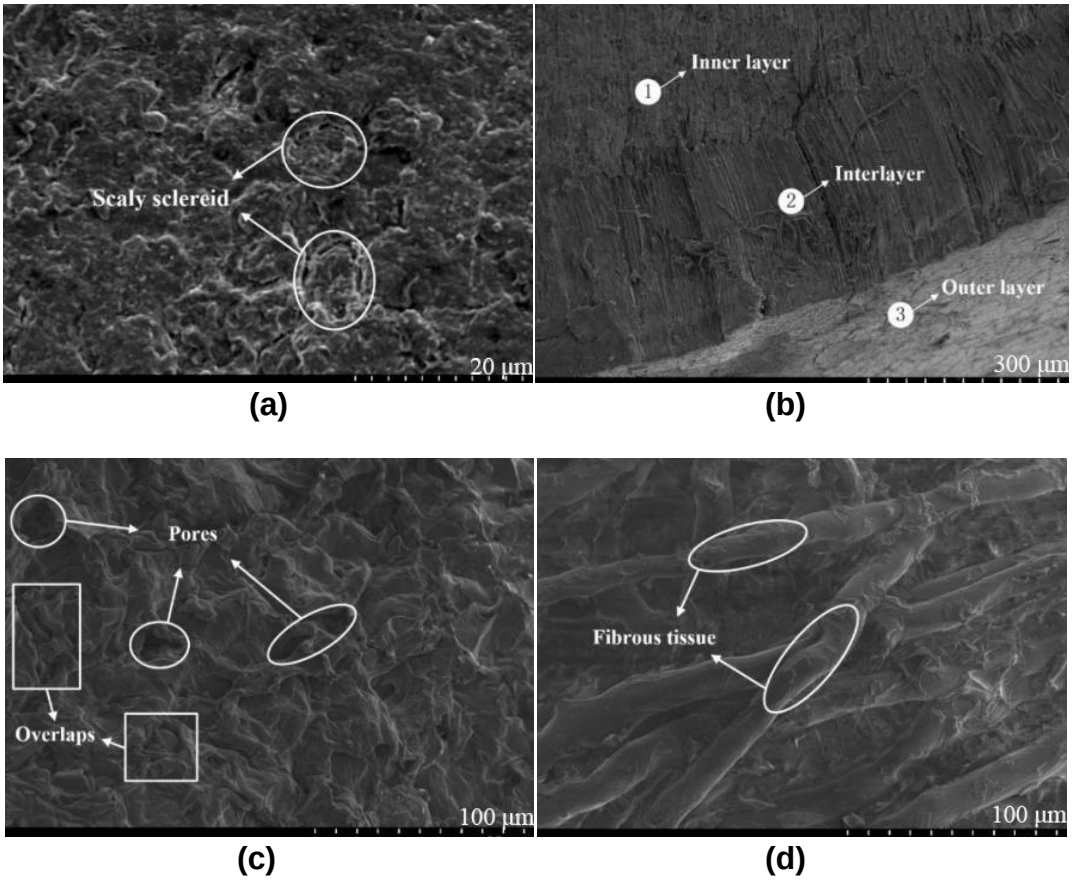

Fig. 10. Microstructure of seed shell: a) outside surface, b) cross-section, c) inner surface, and d) hilum

The cross-section of seed shell can be roughly divided into three layers that become looser and weaker from the outer layer to the inner layer, which may explain the material nonlinearity proposed in the analysis and discussion of the elasticity modulus (Fig. 10b). The inner surface clings to the soft and fragile kernel and protects the core directly. It has a more porous structure, with larger flake-like cells and pores and unordered overlaps within the cell arrangement, providing its brittleness and fragility (Fig. 10c). The hilum is situated at the top of the seed and covered by white hair. It has an idiosyncratic fibrous structure is the area with lowest strength and stiffness in the seed shell (Fig. 10d).

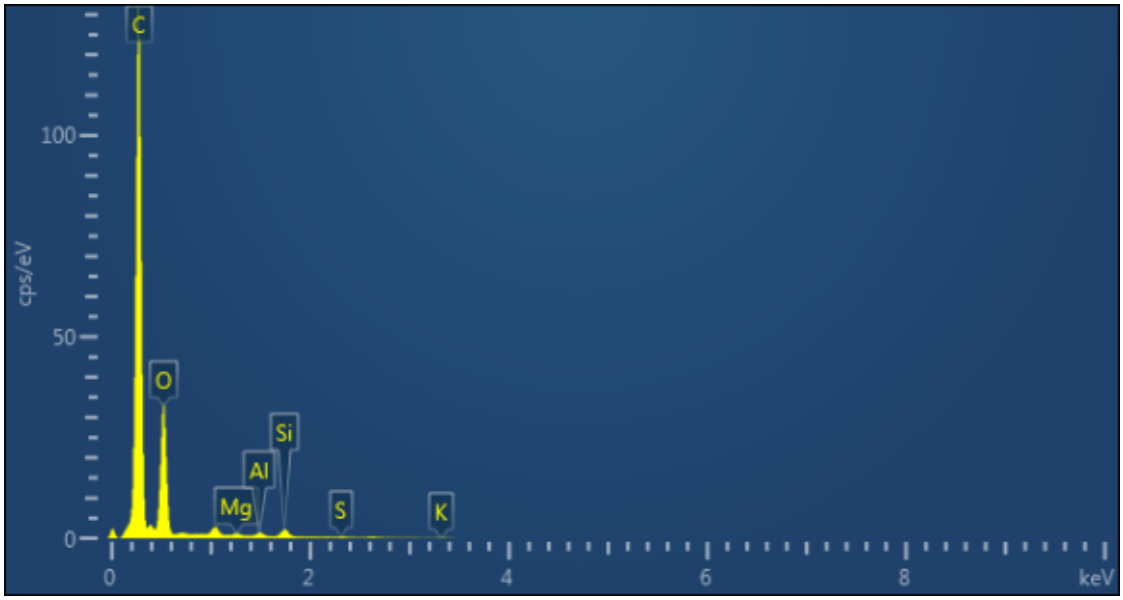

Fig. 11. Energy spectrum of the seed shell

Table 2. Apparent Concentration, Weight Percentage, Atomic Percentage, and Standard Sample of Each Element

Element Name	Apparent Concentration (wt%*)	Weight Percent (wt%)	Atomic Percent (wt%)	Standard Sample
C	42.54	70.00	77.34	Pure element
O	11.94	24.17	20.05	SiO_2
Mg	0.32	0.53	0.29	MgO
Al	0.54	0.90	0.44	Al_2O_3
Si	1.62	2.65	1.25	SiO_2
S	0.22	0.42	0.17	FeS_2
K	0.59	1.34	0.45	KBr
Total	/	100	100	/

*Percentage by weight: wt%

According to the energy spectrum obtained in EDS, the major elements of seed shell included C, O, Si, Mg, Al, K, and S, among which C and O, which are involved in the synthesis of various organic compounds, accounted for more than 90% of the sample by weight. Figure 11 and Table 2 present the percentage and content of each element. Si, which induces the production of lignin and increases the mechanical strength of the cell wall, has a higher proportion than most of the other elements and accounts for 2.65% of the sample by weight. Zhao *et al.* (2021) found that Si enhances the stem strength by promoting lignin accumulation. This phenomenon is explained by the fact that Si increases lignin biosynthetic enzyme activities and gene expression (Zhao *et al.* 2021). The transportation of nutrients and water depends greatly on the hilum, and potassium is important in maintaining the balance of water and salt. Mg and Al, in forming the indispensable cations Mg^{2+} and Al^{3+} in cells, also participate in the synthesis of proteins and bone tissue, whereas S is a major component of FeS protein.

CONCLUSIONS

To analyze the mechanical and physical properties of *S. mukorossi* seed, a method of combining the FEM with experiment data was proposed to measure the density and Poisson ratio of a hollow-sphere seed hull, and the modulus of elasticity was derived from a mechanics formulation. Adopting this method and conducting mesostructure and elemental analyses, this study provided a fundamental understanding of and a reference for the mechanical properties of *S. mukorossi* seeds. The results of the study are summarized as follows.

1. The density of the *S. mukorossi* seed shell was 1.49×10^3 kg/m^3, whereas that of the kernel was 1.07×10^3 kg/m^3, which suggests the possibility of separation.
2. The simulation results showed nearly no lateral deformation of the *S. mukorossi* seed. The deformation of the seed shell during compression was greater on both sides of the seed than in the central area whereas there were distributed areas of greater deformation in the central area.
3. The trends in the simulation results were roughly consistent with those in the experimental data. Moreover, the modulus of elasticity decreased from 1.3 to 0.3 GPa as compression progressed, with the rate of reduction decreasing gradually.
4. Based on the mesostructure of the cross-section, the authors ascribed the material nonlinearity, which reduced elasticity modulus, to the three-layer structure and the tendency of being more compact from the inside to the outside. The seed shell was rich in C and O and also contained a certain amount of Si; these elements relate to physical and mechanical properties of the shell.

ACKNOWLEDGMENTS

The authors are grateful for financial support from Fundamental Research Funds for the Central Universities, grant no. BLX202127; National Natural Science Foundation of China, grant no. 52206229; financial support from the National Key Research and Development Program, grant no. 2019YFD1002401; and financial support from the Graduate Tutor Team of Beijing Forestry University, grant no. YJSY-DSTD202200.

REFERENCES CITED

Abbaspour-Fard, M. H., Khodabakhshian, R., Emadi, B., and Sadrnia, H. (2012). "Evaluation the effects of some relevant parameters on elastic modulus of pumpkin seed and its kernel," *Int. J. Biomater*. 2012, article 271650. DOI: 10.1155/2012/271650

Alimirzaei, S., Mohammadimehr, M., and Tounsi, A. (2019). "Nonlinear analysis of viscoelastic micro-composite beam with geometrical imperfection using FEM: MSGT electro-magneto-elastic bending, buckling and vibration solutions," *Structural Engineering & Mechanics* 71(5), 485-502. DOI: 10.12989/sem.2019.71.5.485

Basu, A., Basu, S., Bandyopadhyay, S., and Chowdhury, R. (2015). "Optimization of vaporative extraction of natural emulsifier cum surfactant from *Sapindus mukorossi*-

characterization and cost analysis," *Industrial Crops and Products* 77, 920-931. DOI: 10.1016/j.indcrop.2015.10.006

Chakraborty, M., and Baruah, D. C. (2013). "Production and characterization of biodiesel obtained from *Sapindus mukorossi* kernel oil," *Energy* 60, 159-167. DOI: 10.1016/j.energy.2013.07.065

Cotabarren, I., Schulz, P. G., Bucalá, V., and Piña, J. (2008). "Modeling of an industrial double-roll crusher of a urea granulation circuit," *Powder Technology* 183(2), 224-230. DOI: 10.1016/j.powtec.2007.07.023

Cuong-Le, T., Nguyen, K. D., Le-Minh, H., Phan-Vu, P., Nguyen-Trong, P., and Tounsi, A. (2022). "Nonlinear bending analysis of porous sigmoid FGM nanoplate via IGA and nonlocal strain gradient theory," *Advances in Nano Research* 12(5), 441-455. DOI: 10.12989/anr.2022.12.5.441

de Figueiredo, A. K., Baümler, E., Riccobene, I. C., and Nolasco, S. M. (2011). "Moisture-dependent engineering properties of sunflower seeds with different structural characteristics," *Journal of Food Engineering* 102(1), 58-65. DOI: 10.1016/j.jfoodeng.2010.08.003

Fabiana, R. G., Souza, L. A., Milaneze-Gutierre, M. A., and Almeida, O. J. G. (2016). "Seed structure and *in vitro* seedling development of certain Laeliinae species (Orchidaceae)," *Revista Mexicana de Biodiversidad* 87(1), 68-73. DOI: 10.1016/j.rmb.2016.01.005

Fan, Q. Y., Chai, C. C., Wei, Q., and Yang, Y. T. (2017). "Thermodynamic, elastic, elastic anisotropy and minimum thermal conductivity of β -GaN under high temperature," *Chinese Journal of Physics* 55(2), 400-411. DOI: 10.1016/j.cjph.2017.01.007

Garg, A., Belarbi, M.-O., Tounsi, A., Li, L., Singh, A., and Mukhopadhyay, T. (2022). "Predicting elemental stiffness matrix of FG nanoplates using Gaussian Process Regression based surrogate model in framework of layerwise model," *Engineering Analysis with Boundary Elements* 143, 779-795. DOI: 10.1016/j.enganabound.2022.08.001

Hamouda, T., Seyam, A.-F. M., and Peters, K. (2015). "Evaluation of the integrity of 3D orthogonal woven composites with embedded polymer optical fibers," *Composites Part B: Engineering* 78, 79-85. DOI: 10.1016/j.compositesb.2015.03.092

Kogut, L., and I. Etsion. (2002). Elastic-plastic contact analysis of a sphere and a rigid flat. *Journal of Applied Mechanics*, 69(5): 657-662. DOI: 10.1115/1.1490373

Kumar, Y., Gupta, A., and Tounsi, A. (2021). "Size-dependent vibration response of porous graded nanostructure with FEM and nonlocal continuum model," *Advances in Nano Research* 11(1), 1-17. DOI: 10.12989/anr.2021.11.1.001

Kwon, J., Cho, H. C., Mun, M., and Kim, K. (2012). "Modeling of coal breakage in a double-roll crusher considering the reagglomeration phenomena," *Powder Technology* 232, 113-123. DOI: 10.1016/j.powtec.2012.08.021

Liu, Z. Z., Gui, M. L., Xu, T. T., Zhang, L., Kong, L. G., Qin, L., and Zou, Z. R. (2019). "Efficient aqueous enzymatic-ultrasonication extraction of oil from *Sapindus mukorossi* seed kernels," *Industrial Crops and Products* 134, 124-133. DOI: 10.1016/j.indcrop.2019.03.065

Morikawa, T., Xie, Y. Y., Ninomiya, K., Okamoto, M., Muraoka, O., Yuan, D., Yoshikawa, M., and Hayakawa, T. (2010). "Inhibitory effects of acylated acyclic sesquiterpene oligoglycosides from the pericarps of *Sapindus rarak* on tumor necrosis

factor-α-induced cytotoxicity," *Chemical and Pharmaceutical Bulletin* 58(9), 1276-1280. DOI: 10.1248/cpb.58.1276

Munder, S., Argyropoulos, D., and Müller, J. (2017). "Class-based physical properties of air-classified sunflower seeds and kernels," *Biosystems Engineering* 164, 124-134. DOI: 10.1016/j.biosystemseng.2017.10.005

Peterka, J., and Buranský, I. (2011). "Using ARAMIS for measurement of deformation of thin-walled parts during milling," *Research Papers Faculty of Materials Science and Technology Slovak University of Technology* 18(28), 45-50. DOI: 10.2478/v10186-010-0005-3

Santalla, E. M., and Mascheroni, R. H. (2003a). "Equilibrium moisture characteristics of high oleic sunflower seeds and kernels," *Drying Technology* 21(1), 147-163. DOI: 10.1081/DRT-120017288.

Santalla, E. M., and Mascheroni, R. H. (2003b). "Note: Physical properties of high oleic sunflower seeds," *Food Science and Technology International* 9(6), 435-442. DOI: 10.1177/1082013203040756

Selvam, T. A., Manikantan, M. R., Chand, T., Sharma, R., and Seerangurayar, T. (2014). "Compression loading behaviour of sunflower seeds and kernels," *International Agrophysics* 28(4), 543-548. DOI: 10.2478/intag-2014-0045

Shah, M., Parveen, Z., and Khan, M. R. (2017). "Evaluation of antioxidant, anti-inflammatory, analgesic and antipyretic activities of the stem bark of *Sapindus mukorossi*," *BMC Complementary and Alternative Medicine* 17, article no. 526. DOI: 10.1186/s12906-017-2042-3

Sun, C. W., Jia, L. M., Xi, B. Y., Wang, L. C., and Weng, X. H. (2017). "Natural variation in fatty acid composition of *Sapindus* spp. seed oils," *Industrial Crops and Products* 102, 97-104. DOI: 10.1016/j.indcrop.2017.03.011

Sunanda, Tiwari, D. P., Sharma, D. N., and Kumar, R. T. S. (2013). "*Sapindus* based activated carbon by chemical activation," *Research Journal of Material Sciences* 1(7), 9-15.

Tu, C., Yang, W., Yin, Q. J., and Lü, J. L. (2015). "Optimization of technical parameters of breaking macadamia nut shell and finite element analysis of compression characteristics," *Transactions of the CSAE* 31(16), 272-277.

Van Vinh, P., Van Chinh, N., and Tounsi, A. (2022). "Static bending and buckling analysis of bi-directional functionally graded porous plates using an improved first-order shear deformation theory and FEM," *European Journal of Mechanics - A/Solids* 96, article 104743. DOI: 10.1016/j.euromechsol.2022.104743

Wang, X., Zhang, R. G., Yun, Q. Z., Xu, Y. Y., Zhao, G. C., Liu, J. M., Shi, S. L., Chen, Z., and Jia, L. M. (2021). "Comprehensive analysis of complete mitochondrial genome of *Sapindus mukorossi* Gaertn.: An important industrial oil tree species in China," *Industrial Crops and Products* 174, article ID 114210. DOI: 10.1016/j.indcrop.2021.114210

Yekeen, N., Malik, A. A., Idris, A. K., Reepei, N. I., and Ganie, K. (2020). "Foaming properties, wettability alteration and interfacial tension reduction by saponin extracted from soapnut (*Sapindus mukorossi*) at room and reservoir conditions," *Journal of Petroleum Science and Engineering* 195, article ID 107591. DOI: 10.1016/j.petrol.2020.107591

Yin, S. W., Chen, J. C., Sun, S. D., Tang, C. H., Yang, X. Q., Wen, Q. B., and Qi, J. R. (2011). "Physicochemical and structural characterisation of protein isolate, globulin and albumin from soapnut seeds (*Sapindus mukorossi* Gaertn.)," *Food Chemistry* 128(2), 420-426. DOI: 10.1016/j.foodchem.2011.03.046

Zhao, D., Xu, C., Luan, Y., Shi, W., Tang, Y., and Tao, J. (2021). "Silicon enhances stem strength by promoting lignin accumulation in herbaceous peony (*Paeonia lactiflora* Pall.)," *Int. J. Biol. Macromol*. 190, 769-779. DOI: 10.1016/j.ijbiomac.2021.09.016

Article submitted: July 24, 2022; Peer review completed: September 18, 2022; Revised version received and accepted: December 1, 2022; Published: December 8, 2022.
DOI: 10.15376/biores.18.1.1008-1024